SIRM 2015 – 11th International Conference on Vibrations in Rotating Machines,
Magdeburg, Germany, 23. – 25. February 2015

High Speed Hydrodynamic Journal Bearings – State of the Art of Calculations

Andreas Fuchs [1], **Joachim Schmied** [2], **Alexander Kosenkov** [3]

[1] Delta JS AG, 8005, Zürich, Switzerland, afuchs@delta-js.ch
[2] Delta JS AG, 8005, Zürich, Switzerland, jschmied@delta-js.ch
[3] Delta JS AG, 8005, Zürich, Switzerland, alexander.kosenkov@delta-js.ch

Abstract

The operating behaviour and thereby the unsteady bearing load of high speed hydrodynamic bearings can be affected by dynamic effects in the oil supply, the energetic coupling of the oil films and tolerances in the lubricating gap. The 2D oil film pressure, the 3D temperature distribution in the oil film, and the bearing shell as well as the static and dynamic bearing coefficients can be more precisely calculated with the enhanced program ALP3T2Penhanced (considering two phase model and inertia forces in the oil film) compared to classical cavitation models such as Gümbel and Reynolds boundary conditions. This applies to complex sliding bearings with various geometries, with hydrodynamic pockets and to various bearing types, such as tilting pad bearings, floating ring bearings as well as to squeeze film dampers. The modelling of the pad geometry, which is described by curvature radii and centres, is supported by user-friendly Graphical User Interface. The calculation is based on an iterative solution of the extended Reynolds, energy and deformation equations, including temperature and pressure dependent properties of the oil film.

By integrating the program ALP3T2Penhanced into the program-system MADYN 2000, the vibration behaviour of rotor – bearing – basement systems can be accurately calculated. Analysing such systems reveals that the damping in the cavitation areas and the local inertia forces in the lubricating oil films can significantly change the non-linear vibration behaviour of such complex systems. For static non-centred, non-rotating floating ring bearings and squeeze film dampers, the important centring effect due to the dynamic load (actually creating load-carrying capacity) can be clearly shown by non-linear analyses with the enhanced program system.

Nomenclature

B	bearing width
c	lubricant specific heat
c_{ik}	stiffness coefficient
d_{ik}	damping coefficient
D	bearing diameter $2R$
H	film thickness $h/\Delta R$
K_x,K_z	turbulence factors
m	mass
p	pressure
r	journal radius
R	journal bearing radius (inside)
R_S	pad radius
Re	Reynold number $\mathrm{Re}=\rho\omega r\Delta R/\eta$
Re^*	modified Reynolds number $\mathrm{Re}\psi$
So_D	Sommerfeld number for rotation $F_{stat}\psi^2/(BD\eta\omega)$
So_V	Sommerfeld number for squeezing $F_V\psi^2/(BD\eta\omega)$
T	temperature
V	volume of phase
$\bar{y}, \bar{z}$	radial, axial coordinate $\bar{y}=y/\Delta R, \bar{z}=z/r$
u,v,w	flow velocities $u=U/(\omega r),v=V/(\omega\Delta R),w=W/(\omega r)$
α_D	resulting angle of bearing pressure
ΔR	radial bearing clearance $R-r$
γ	attitude angle of journal
δ	tilting angle of pad
ε	relative eccentricity of journal $e/\Delta R$
$\varepsilon_{h,v}$	horizontal, vertical canting of journal $\varepsilon_i=(x,y)/\Delta R$
η	lubricant dynamic viscosity
φ	angular coordinate
ϕ	time ωt
Π	lubricant pressure $p\psi^2/(\eta\omega)$
ρ	density
ψ	relative bearing clearance $\Delta R/R$
ψ_d	relative pad thickness t_P/r
ψ_S	relative pad clearance $(R_S-r)/\Delta R$
τ	center angle of pad radius
ω	journal rotational velocity
ω_S	journal vibration frequency

1 Introduction

For the calculation of the load capacity of multi-lobe and tilting pad bearings normally only insufficient models are used for the energy coupling of the lubricating oil film in circumferential and axial direction [1] – [3]. For floating ring bearings and squeeze film dampers, the energetically coupling of the oil films by the radial heat conduction and oil flow is in general neglected or only considered by rough approaches [4]. These effects can considerably influence the transient bearing capacity and thus the allowable unbalance, the threshold of self-excited vibrations and the load capacity of squeeze film dampers for high velocities.

Therefore an efficient method is presented for calculating the stationary and transient load capacity of general radial journal bearings, floating ring bearings and squeeze film dampers, which takes into account the important "additional effects" for high vibration velocities. By integrating the journal bearing program into a linear and non-linear rotor-dynamic program [5], complex rotor bearing systems can be also calculated for difficult operating conditions.

2 Theory

High friction losses occur in the oil film for high sliding velocities. This leads to high temperature gradients in the lubricating film because of the low heat conductivity of typically used oil types. Therefore extended formulas of the basic equations have to be used for calculating the hydrodynamic pressure in high-speed journal bearings. These formulas must consider the change of the strongly temperature-dependent viscosity of the lubricating oil in all three coordinate directions [3]. Solving the energy equation and the appropriate heat transfer equations leads to three-dimensional temperature distribution of the lubricating film, the bearing bush and the shaft.

Significant simplifications are used in the calculation procedures in [3] in contrast to ALP3T2Penhanced, such as idealized geometry of the bearings, negligence of the thermal and elastic deformations of the bearing bush, symmetrical boundary conditions in axial direction for the calculation of the pressure and temperature distribution, and negligence of the local inertia forces in the lubricating film.

The local film thickness of each lobe or pad can be described by equation (1), see [6]

$$H(\varphi,\bar{z}) = \underbrace{\frac{\psi_S}{\psi} + \left(\frac{\psi_S}{\psi} - 1\right)\cos(\varphi-\tau)}_{\text{curvature of lobe or pad}} + \underbrace{\frac{\delta}{\psi}(1+\psi_d)\sin(\varphi-\tau)}_{\text{tilting of pad}} - \underbrace{\varepsilon\cos(\varphi-\tau)}_{\substack{\text{displacement}\\ \text{of shaft}}} - \underbrace{\bar{z}\frac{\sqrt{\varepsilon_h^2+\varepsilon_v^2}}{B/D}\cos\left(\varphi - \arctan\frac{\varepsilon_h}{\varepsilon_v}\right)}_{\text{misalignment}}. \quad (1)$$

2.1 Two Phase Model for Lubricating Film

It is possible to capture the influence of the air, which is dissolved in the lubricating oil, and the mixture of air and oil in the cavitation area (Figure 1) with a quite simple two-phase flow model. As it is shown by several studies, the air which is solved in the oil does not change the viscosity and the density of the oil very much [7]. In contrast, the viscosity of the oil-air mixture changes noticeably for increasing foaming of the lubricating film. The variation of the viscosity due to the air-oil mixture depends on the diameter and surface tension of the air bubbles and the shear stress in the lubricating gap [7]. In hydrodynamic bearings and squeeze film dampers the following approach can be derived, since the shear stress is usually much bigger than the surface tension of the air bubbles:

$$\eta_{mix} = \eta_{Oil}(1-C) = \eta_{Oil}\frac{V_{total}-V_b}{V_{total}} = \eta_{Oil}\frac{1}{1+r} \quad (2)$$

with $C = V_b/V_{total} = V_b/(V_b+V_{oil})$ degree of foaming, $r = V_b/V_{Oil}$ amount of bubbles.

The relative local density ρ_{mix} depends on the gas diffusing in and out of the oil. It is modelled as a function of the film pressure. The undissolved air arises as bubbles in the oil. The ratio r between the undissolved gas and the oil can be calculated by use of the Henry-Daltons and Boyle-Mariottes law:

$$r = r_0\frac{T\,p_0}{T_0\,p} - a_v\frac{T_0\,p - p_0\,T}{T_0\,p}, \quad (3)$$

with p = absolute pressure, T = absolute temperature in Kelvin and index 0 = ambient conditions. By neglecting the mass of the undissolved air the relative local density is

$$\rho_{mix} = \frac{m_{Oil} + m_b}{V_{Oil} + V_b} \approx \rho_{Oil}\frac{1}{1+r}. \quad (4)$$

The Bunsen-Coefficient is $a_v \approx 0.08 \ldots 0.09$ for relevant mineral oils (ISO-VG 32 to ISO-VG 220) and is nearly independent of the temperature (T = 20 °C to 100 °C).

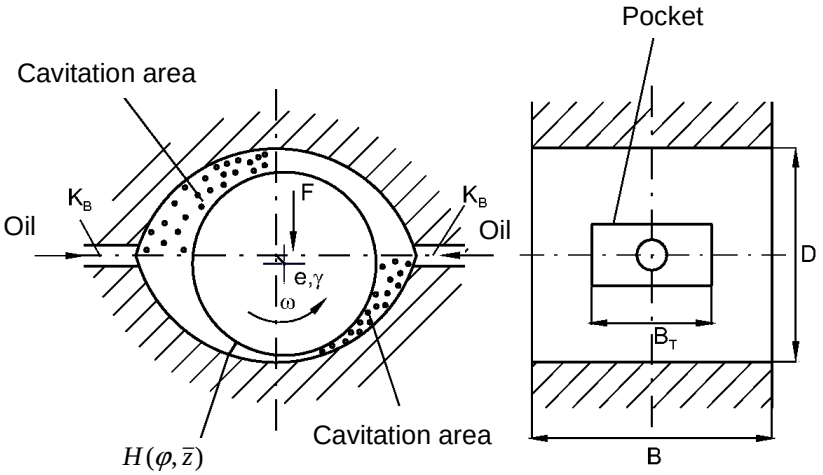

Figure 1: Cavitation areas in a lemon type bearing

2.2 Pressure Distribution in the bearing

The flow can be described in journal bearings by using the Navier-Stokes equations and the continuity equation [9]. These equations can be simplified by use of the common assumptions for the hydrodynamic bearing theory [10]. For the numerical solution procedure these equations are usually transferred in a non-dimensional form:

$$\begin{aligned}
&\mathrm{Re}^*\left\{\frac{\partial(\rho_{mix}u)}{\partial\phi}+\frac{\partial(\rho_{mix}u^2)}{\partial\varphi}+\frac{\partial(\rho_{mix}u\,v)}{\partial\bar{y}}+\frac{\partial(\rho_{mix}u\,w)}{\partial\bar{z}}\right\}=-\frac{\partial\Pi}{\partial\varphi}+\frac{\partial}{\partial\bar{y}}\left[\eta_m^*\left(1+\frac{\eta_t}{\eta_m}\right)\frac{\partial u}{\partial\bar{y}}\right]\\
&\mathrm{Re}^*\left\{\frac{\partial(\rho_{mix}w)}{\partial\phi}+\frac{\partial(\rho_{mix}u\,w)}{\partial\varphi}+\frac{\partial(\rho_{mix}v\,w)}{\partial\bar{y}}+\frac{\partial(\rho_{mix}w^2)}{\partial\bar{z}}\right\}=-\frac{\partial\Pi}{\partial\varphi}+\frac{\partial}{\partial\bar{y}}\left[\eta_m^*\left(1+\frac{\eta_t}{\eta_m}\right)\frac{\partial w}{\partial\bar{y}}\right] \qquad (5)\\
&\frac{\partial\rho_{mix}}{\partial\phi}+\frac{\partial(\rho_{mix}u)}{\partial\varphi}+\frac{\partial(\rho_{mix}v)}{\partial\bar{y}}+\frac{\partial(\rho_{mix}w)}{\partial\bar{z}}=0.\ \text{(Continuity equation)}
\end{aligned}$$

The local inertia forces of the lubricating film are described by the left hand side of the Navier-Stokes equations, while the turbulent flow regime is included in the last term on the right side of the Navier-Stokes equations. The generalized Reynolds equation can be achieved by partial integration of the Navier-Stokes and the continuity equation over the lubricating gap from $\bar{y}=0$ to $\bar{y}=H$ and applying the common boundary conditions for the flow velocity [6]:

$$\begin{aligned}
&\frac{\partial}{\partial\varphi}\left(\frac{H^3}{12\eta_P^*K_x}\frac{\partial\Pi}{\partial\varphi}\right)+\frac{\partial}{\partial\bar{z}}\left(\frac{H^3}{12\eta_P^*K_x}\frac{\partial\Pi}{\partial\bar{z}}\right)=\frac{1}{2}\frac{\partial(\rho_{mix}f_CH)}{\partial\varphi}+\frac{\partial(\rho_{mix}H)}{\partial\phi}+R_1(\varphi,\bar{z})+R_2(\varphi,\bar{z},\phi),\\
&R_1=-\mathrm{Re}^*\left\{\frac{\partial}{\partial\varphi}\left[\frac{H^2}{12\eta_P^*K_x}\left(\frac{\partial}{\partial\varphi}\int_0^H\rho_{mix}u^2d\bar{y}+\frac{\partial}{\partial\bar{z}}\int_0^H\rho_{mix}uwd\bar{y}\right)\right]+\frac{\partial}{\partial\bar{z}}\left[\frac{H^2}{12\eta_P^*K_z}\left(\frac{\partial}{\partial\varphi}\int_0^H\rho_{mix}uwd\bar{y}+\frac{\partial}{\partial\bar{z}}\int_0^H\rho_{mix}w^2d\bar{y}\right)\right]\right\} \qquad (6)\\
&R_2=\mathrm{Re}^*\left\{\frac{H^2}{12\eta_P^*}\frac{\partial^2H}{\partial\phi^2}-\frac{\partial}{\partial\phi}\int_0^H\rho_{mix}ud\bar{y}\,\frac{\partial}{\partial\varphi}\left(\frac{H^2}{12\eta_P^*}\right)-\frac{\partial}{\partial\phi}\int_0^H\rho_{mix}wd\bar{y}\,\frac{\partial}{\partial\bar{z}}\left(\frac{H^2}{12\eta_P^*}\right)\right\}
\end{aligned}$$

$R_1(\varphi,\bar{z})$ represents the convective inertia forces, while $R_2(\varphi,\bar{z},\phi)$ gives the inertia forces due to acceleration. The factors η_P^* and f_C includes the local distribution of the viscosity. These factors change in circumferential and axial direction. The local turbulent flow regime is included in equation (6) by the correcting factors K_x and K_z. Turbulent flow occurs, if the local Reynolds number $\mathrm{Re}_l=\rho_{mix}r\omega H/\eta$ is bigger than the critical Reynolds number Re_{cr}. The factors K_x and K_z can be calculated by using empirical equations [3].

By taking the oil foaming and the local inertia forces into account the pure Poiseuille flow remains nearly unchanged in the Reynolds equation (6) in comparison to [3], while the Couette flow will be changed and additional source terms occur for the pressure generation in the lubricating film. These effects are not included in the simple DIN calculation [2], for example.

For solving the Reynolds equation, the pressure at the edges of the pads is set to the ambient pressure Π_0 or to the pressure of the hydrostatic pocket Π_T. Additional boundary conditions at the beginning or the end of the cavitation area are not necessary in the model shown here. The pocket pressure Π_T can be calculated by means of the law of mass conservation with applied flow factors for the oil supply and resistance factors of the pocket. The resistance factor R_T of the pocket is the sum of a viscosity and density proportional resistance $R_T = R_{\eta T} + R_{\rho T}$. The Reynolds equation is solved together with the boundary conditions, the equations for the mass balance, for the fluid flow, for the local film thickness and the correction factor for turbulent flow using a finite volume method with the improved SLOR solver [3], [6]. The two-dimensional pressure distribution $\Pi(\varphi, \bar{z})$ is the result of the numerical solution for the steady state part of the Reynolds equation,

Figure 2 shows a comparison between the measured and calculated pressure distributions for a pressure dam bearing. Significant deviations occur to the measured pressure distribution if the oil foaming and the local inertia forces are not considered (ALP3T [3]). Indeed, the pressure distribution, which has been calculated with ALP3T2Penhanced, matches quite well to the measured values by taking the local convective inertia forces into account. The remaining deviations can be explained by a small ovality of the split bearing bushes or a smaller effective clearance during the measurements.

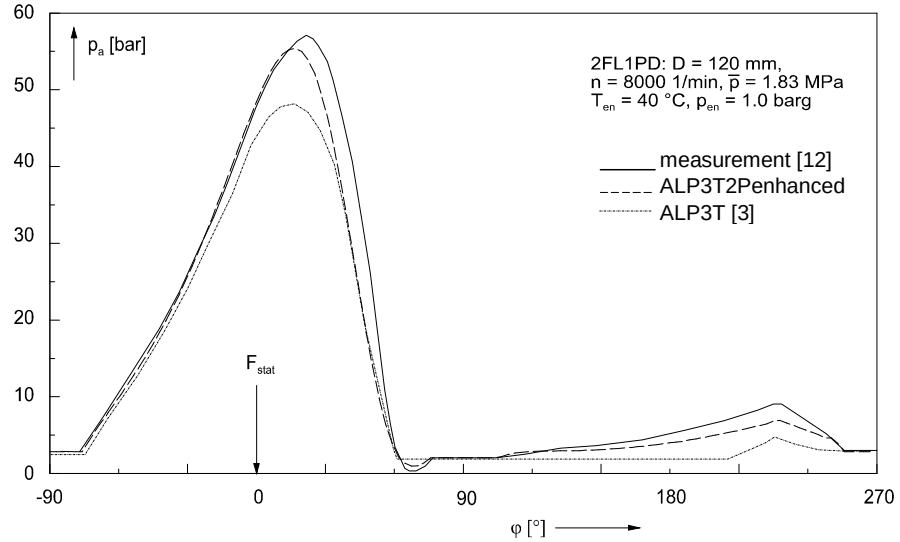

Figure 2: Pressure distribution in a pressure dam bearing

2.3 Temperature Distribution in the bearing

The steady state, 3D temperature distribution $T(\varphi, y, \bar{z})$ can be calculated in the lubricating gap by the energy equation for compressible flow:

$$\operatorname{div}(\rho c \vec{u} T) = \operatorname{div}(\lambda \operatorname{grad} T) + \eta \Phi, \quad \Phi = \left(\frac{\partial u}{\partial y}\right)^2 + \left(\frac{\partial w}{\partial y}\right)^2 . \tag{7}$$

Here, the dissipation Φ is reduced to the most dominant velocity gradients. The approach of Falz [11] is used for calculating the viscosity η as a function of the temperature ($\eta / \eta_0 = (T / T_0)^{-l}$). The turbulent flow regime is also included by improved heat conductivity and the eddy viscosity of the oil film.

The Reynolds (6) and the energy equation (7) are nonlinearly-coupled by the physical properties of the oil (viscosity and density). Therefore both equations must be solved simultaneously in an iteration process [6]. The hot-cold-oil mixing in the pockets and the heat conductivity equations (for the bearing bush and the shaft) must also be considered. The 2D or 3D heat conductivity equations are used for the calculation of the temperature distribution in the bearing bush and in the shaft, respectively:

$$\begin{aligned} &\text{for the bearing bush} && \Delta T_B(\varphi, z, r) = 0 \\ &\text{for the shaft} && \Delta T_S(z, r) = 0 \end{aligned} \qquad \Delta: \text{Laplace operator} . \tag{8}$$

2.4 Bearing Characteristics

The static bearing properties, such as bearing load, power loss or oil flow, can be calculated by integration of the corresponding pressure distribution, the shear stress and velocity distribution, respectively, on their corresponding surfaces, if the bearing profile $H(\varphi, \bar{z})$, B / D), the displacement of the shaft (ε, γ) and additional parameter (T_{en}, p_{en}, η_{en}, K_B, ρ, λ, α, …) are given.

The transient bearing (F_x, F_y) load can be linearly approximated by means of stiffness and damping coefficients (c_{ik}, d_{ik}) for small vibrations of the shaft [2], [3], [13]:

$$\begin{bmatrix} F_x \\ F_y \end{bmatrix} = \begin{bmatrix} 0 \\ F_{stat} \end{bmatrix} + \begin{bmatrix} c_{11} & c_{12} \\ c_{21} & c_{22} \end{bmatrix} \begin{bmatrix} x \\ y \end{bmatrix} + \begin{bmatrix} d_{11} & d_{12} \\ d_{21} & d_{22} \end{bmatrix} \begin{bmatrix} \dot{x} \\ \dot{y} \end{bmatrix}. \tag{9}$$

With aid of these coefficients, it is possible to analyse the vibration behaviour of a rotor supported on hydrodynamic journal bearing in a linear approach. The stability threshold and the system damping are especially important.

Dynamic coefficients are based on a perturbation of the extended generalized Reynolds equation (6) with the assumption, that shaft experiences only small deflections (X, Y) and velocities ($\dot{X}$, $\dot{Y}$) around the static position of equilibrium (ε, γ_{stat}. Therefore the inertia forces are neglected, as the modified Reynolds number Re^* remains small.

The perturbed variables are the pressure Π and the lubricating gap H, while the density and the temperature are not disturbed (the changes of these variables is assumed to be negligible for small perturbations).

$$\begin{aligned} H(\varphi,\bar{z}) &= H_{stat}(\varphi,\bar{z}) - X\cdot\sin\varphi - Y\cdot\cos\varphi, \\ \frac{\partial H(\varphi,\bar{z})}{\partial\phi} &= -X'\cdot\sin\varphi - Y'\cdot\cos\varphi, \qquad '=\frac{\partial}{\partial\phi}=\frac{\partial}{\partial\omega t} \\ \Pi(\varphi,\bar{z}) &= \Pi_{stat}(\varphi,\bar{z}) + \left(\frac{\partial\Pi}{\partial X}\right)_{stat} X + \left(\frac{\partial\Pi}{\partial Y}\right)_{stat} Y + \left(\frac{\partial\Pi}{\partial X'}\right)_{stat} X' + \left(\frac{\partial\Pi}{\partial Y'}\right)_{stat} Y' \end{aligned} \tag{10}$$

Substituting these expression in equation (6) and sorting the terms according to the first perturbation order (X, Y, X', Y') yields

$$\begin{aligned} &\frac{\partial}{\partial\varphi}\left[\frac{H_{stat}^3}{12\eta_P^* K_x}\frac{\partial}{\partial\varphi}\left(\frac{\partial\Pi}{\partial X}\right)_{stat}\right] + \frac{\partial}{\partial\bar{z}}\left[\frac{H_{stat}^3}{12\eta_P^* K_z}\frac{\partial}{\partial\bar{z}}\left(\frac{\partial\Pi}{\partial X}\right)_{stat}\right] = \\ &\qquad = -\frac{1}{2}\frac{\partial(\rho_{mix} f_C \sin\varphi)}{\partial\varphi} + \frac{\partial}{\partial\varphi}\left[\frac{3H_{stat}^2}{12\eta_P^* K_x}\frac{\partial\Pi_{stat}}{\partial\varphi}\right] + \frac{\partial}{\partial\bar{z}}\left[\frac{3H_{stat}^2}{12\eta_P^* K_z}\frac{\partial\Pi_{stat}}{\partial\bar{z}}\right], \\ &\frac{\partial}{\partial\varphi}\left[\frac{H_{stat}^3}{12\eta_P^* K_x}\frac{\partial}{\partial\varphi}\left(\frac{\partial\Pi}{\partial Y}\right)_{stat}\right] + \frac{\partial}{\partial\bar{z}}\left[\frac{H_{stat}^3}{12\eta_P^* K_z}\frac{\partial}{\partial\bar{z}}\left(\frac{\partial\Pi}{\partial Y}\right)_{stat}\right] = \\ &\qquad = -\frac{1}{2}\frac{\partial(\rho_{mix} f_C \cos\varphi)}{\partial\varphi} + \frac{\partial}{\partial\varphi}\left[\frac{3H_{stat}^2}{12\eta_P^* K_x}\frac{\partial\Pi_{stat}}{\partial\varphi}\right] + \frac{\partial}{\partial\bar{z}}\left[\frac{3H_{stat}^2}{12\eta_P^* K_z}\frac{\partial\Pi_{stat}}{\partial\bar{z}}\right], \\ &\frac{\partial}{\partial\varphi}\left[\frac{H_{stat}^3}{12\eta_P^* K_x}\frac{\partial}{\partial\varphi}\left(\frac{\partial\Pi}{\partial X'}\right)_{stat}\right] + \frac{\partial}{\partial\bar{z}}\left[\frac{H_{stat}^3}{12\eta_P^* K_z}\frac{\partial}{\partial\bar{z}}\left(\frac{\partial\Pi}{\partial X'}\right)_{stat}\right] = -\rho_{mix}\cdot\sin\varphi, \\ &\frac{\partial}{\partial\varphi}\left[\frac{H_{stat}^3}{12\eta_P^* K_x}\frac{\partial}{\partial\varphi}\left(\frac{\partial\Pi}{\partial Y'}\right)_{stat}\right] + \frac{\partial}{\partial\bar{z}}\left[\frac{H_{stat}^3}{12\eta_P^* K_z}\frac{\partial}{\partial\bar{z}}\left(\frac{\partial\Pi}{\partial Y'}\right)_{stat}\right] = -\rho_{mix}\cdot\cos\varphi. \end{aligned} \tag{11}$$

All implicit dependencies of other parameters and boundary conditions have to be linearized for the solution of these four perturbation equations as well. This requires the application of an iterative numerical solution procedure. Due to the two-phase model, no additional boundary conditions are necessary at the beginning and the end of the cavitation areas. The four stiffness ($c_{ik} = \gamma_{ik}^*(2B\eta\omega)/\psi^3$) and damping coefficients ($\omega_S d_{ik} = \beta_{ik}^*(2B\eta\omega)/\psi^3$) can be calculated by integration of the pressure coefficients $\partial\Pi/\partial q_n$ over the whole bearing surface:

$$\begin{aligned} \gamma_{ik}^* &= \frac{1}{4\frac{B}{D}}\int_0^{2\pi}\int_{-B/D}^{B/D}\left(\frac{\partial\Pi}{\partial q_k}\right)\left((i-1)\cos\varphi-(i-2)\sin\varphi\right)\mathrm{d}\bar{z}\,\mathrm{d}\varphi, \\ \beta_{ik}^* &= \frac{1}{4\frac{B}{D}}\int_0^{2\pi}\int_{-B/D}^{B/D}\left(\frac{\partial\Pi}{\partial q_{k+2}}\right)\left((i-1)\cos\varphi-(i-2)\sin\varphi\right)\mathrm{d}\bar{z}\,\mathrm{d}\varphi \end{aligned} \tag{12}$$

with i, k = 1, 2 and $q_n = X, Y, X', Y'$ for n = 1 … 4. The dynamic bearing coefficients γ_{ik}^*, β_{ik}^* depend mainly on the static point of equilibrium of the shaft ($\varepsilon,\gamma_{stat}$, the bearing profile, the function or the film-thickness and the bearing width ratio.

The transient bearing forces have to be nonlinearly calculated for high vibration amplitudes. In the here presented calculation method for calculating the transient bearing forces, the additional effects, which cause long computation times, are only taken into account by averaging. The transient bearing forces are split into two parts, which are proportional to the rotation and lateral movements. The bearing force corresponds to the static bearing force [So_D, α_D]. The damping force depends linearly on the shaft moving velocity (ε', γ') according to the journal bearing theory [3] and it can be described by the use of the damping coefficients β_{ik}^* . The coefficients depend in a highly nonlinear way on the actual position of the shaft (ε, γ) in the bearing, as well as on the bearing force [So_D, α_D].

$$\begin{bmatrix} \overline{\Pi}_x \\ \overline{\Pi}_y \end{bmatrix} = \begin{bmatrix} So_D \sin\alpha_D \\ So_D \cos\alpha_D \end{bmatrix}_{\varepsilon,\gamma} + \begin{bmatrix} \beta_{11}^* & \beta_{12}^* \\ \beta_{21}^* & \beta_{22}^* \end{bmatrix}_{\varepsilon,\gamma} \begin{bmatrix} X' \\ Y' \end{bmatrix}. \tag{13}$$

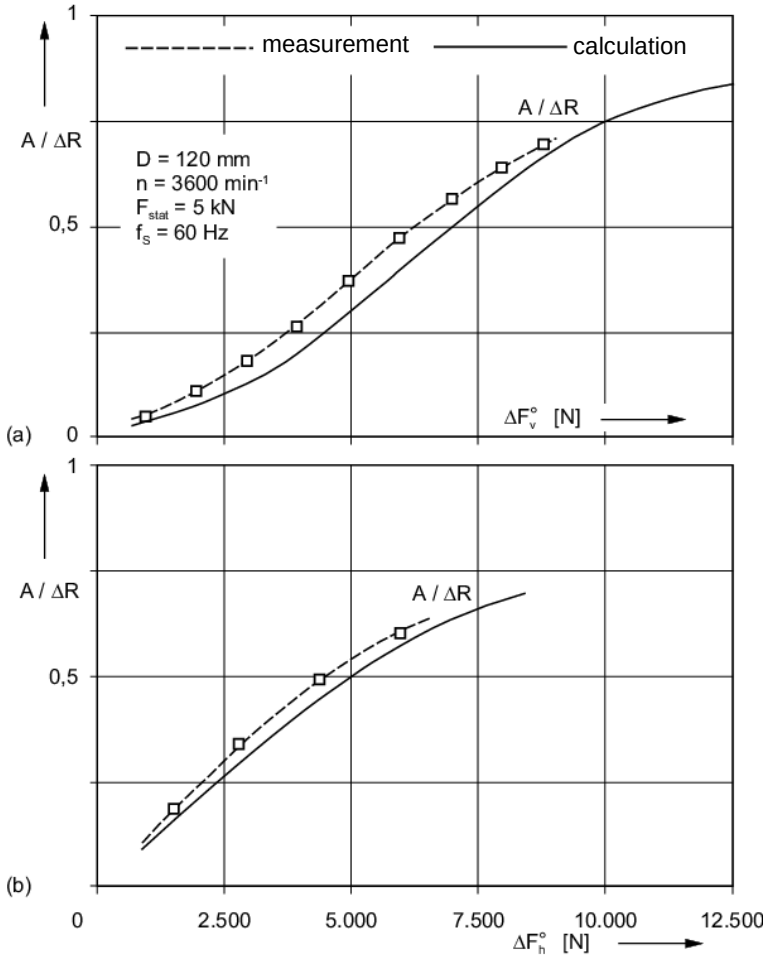

Figure 3: Measured and calculated vibration amplitudes

For the calculation of the bearing coefficients (So_D, α_D, β_{ik}^*) with the program ALP3T2Penhanced, necessary inputs are the bearing geometry, oil parameters, temperature and pressure boundary conditions, material parameters as well as parameters for the two-phase model. The coefficients are tabulated as a function of the shaft displacement (ε, γ) for the whole possible shaft positions in the bearing. The reliability of the transient bearing force calculation has been proven by several measurements [14] on a bearing test rig, Figure 3.

3 Calculation Results for Hydrodynamic Journal Bearings

3.1 Closed Bearings

The journal bearing program ALP3T2Penhanced has been integrated into the rotor dynamics program MADYN 2000 [5]. A user friendly GUI (Figure 4) has been implemented in order to simplify and reduce the necessary input data.

With the enhanced program ALP3T2Penhanced, it is also possible to calculate closed bearings without hydrostatic pockets. The oil flow through the bearing is in axial direction.

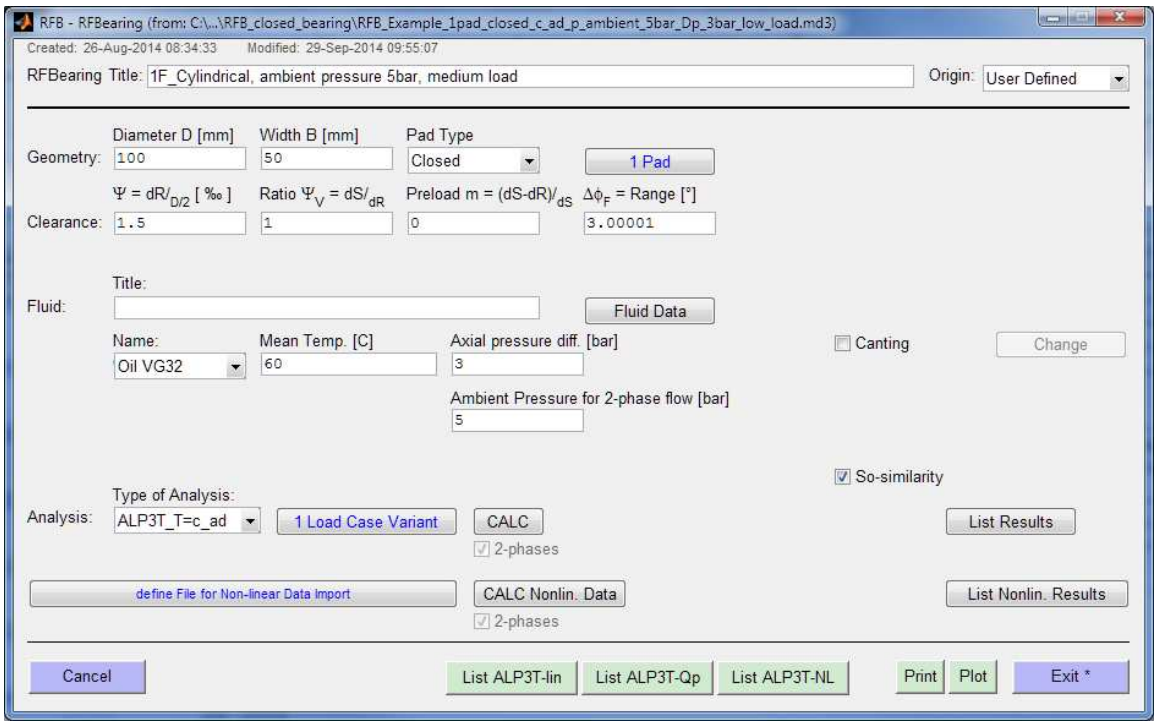

Figure 4: User-friendly GUI for ALP3T2PT for a closed bearing

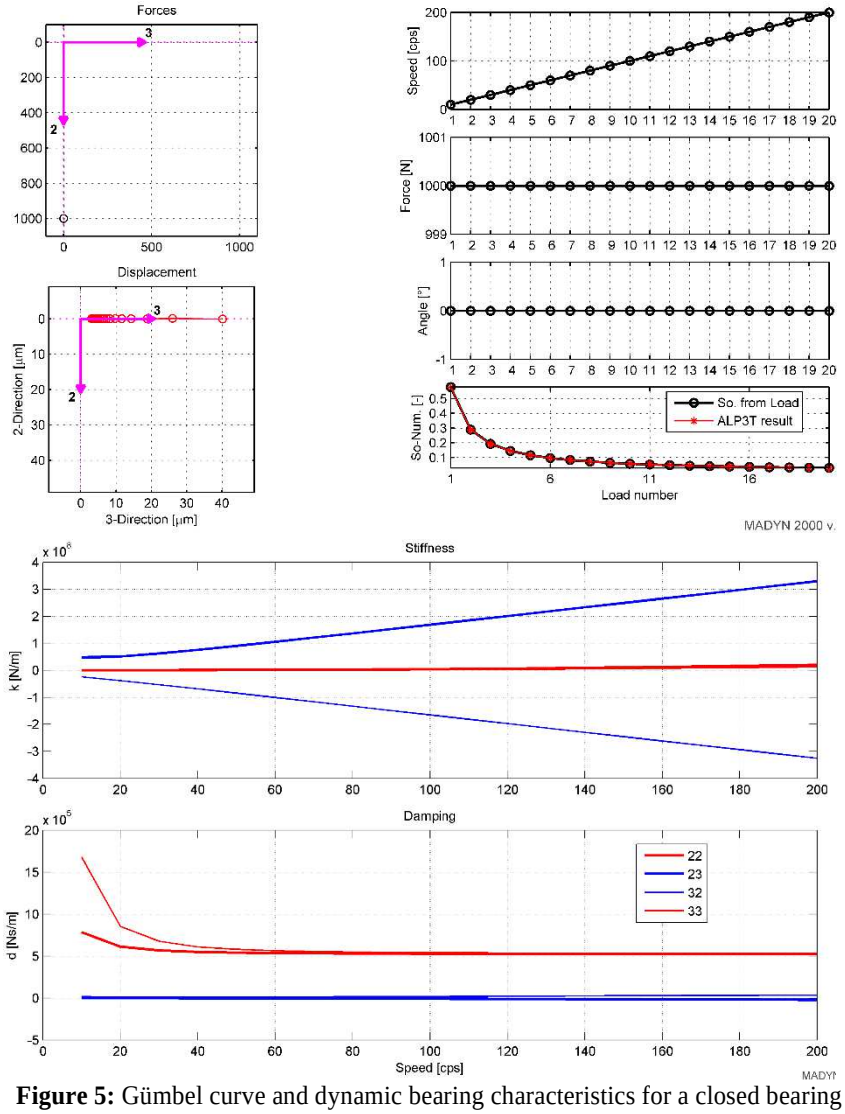

Figure 5: Gümbel curve and dynamic bearing characteristics for a closed bearing

The calculation results of a closed bearing are shown in Figure 5. The Gümbel curve is plotted in the upper figures. The shaft deflects perpendicularly to the load direction, which means the angle between the load- and deflection direction is 90°. This is due to the fact that no cavitation occurs is the bearing because of the moderate bearing load of 2 bar and the axial pressure difference of 3 bar between both axial bearing ends. Such bearing is prone to become unstable.

In the lower figures the dimensioned stiffness- (*k*) and damping (*d*) coefficients are plotted. The main stiffness (22, 33) coefficients and the cross damping (23, 32) coefficients are almost 0, whereas non-zero cross coupling stiffness coefficients (23, 32) and non-zero direct damping coefficients appear. The cross coupling stiffness coefficients are skew symmetric. This is also predicted by the short bearing theory.

3.2 Tilting Pad Bearings

For multi-lobe and tilting pad bearings, the lubricating films are essentially coupled in the circumferential direction by the oil flow into and out of the pockets. Also the heat conduction in the bearing and in the shaft has to be taken into account. The old program ALP3T [3] calculates to high oil flows in the pocket area especially for multi-lobe bearing with a high relative pocket width or open pockets. This yields significant differences in the calculated and measured bearing temperatures due to the hot and cold oil mixture in the pockets. Remarkable improvements could be achieved considering the inertia forces in the lubricating film and the back-flow of oil in cavitation areas.

For tilting pad bearings with limited oil flow, it is not ensured that all pads get sufficient amount of oil for a complete filling of the lubricating gap at the entrance of the pad. To achieve this, the oil drainage must be reduced as long as the hot oil substitutes the missing amount of cold oil. This important energetic coupling of the lubricating films was not implemented in ALP3T, so that there are significant deviations between the measured and calculated pad temperatures, Figure 6a. These differences are much smaller with the new oil mixture model and with consideration of the pad cooling, Figure 6b.

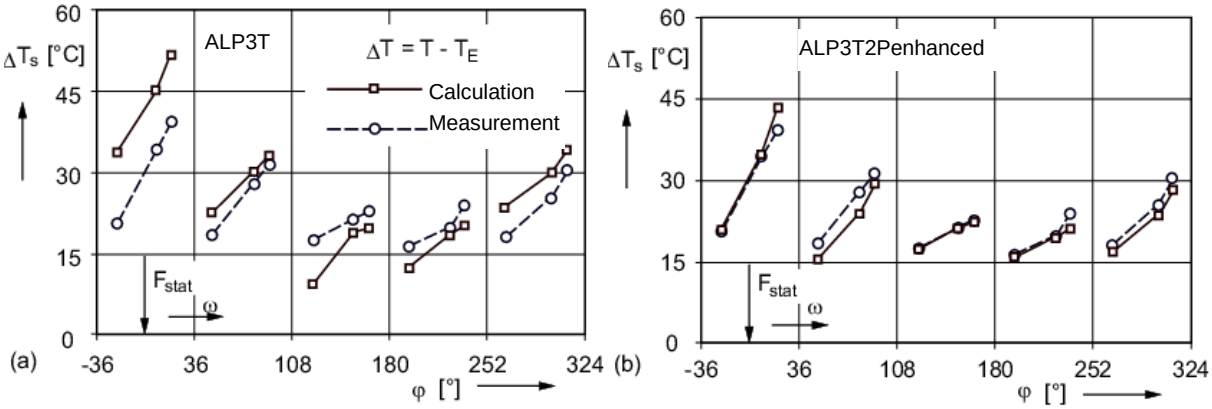

Figure 6: Comparison between measured and calculated temperature distributions T(φ,z)

The program ALP3T2Penhanced is also integrated in MADYN 2000 for nonlinear calculations, which become necessary among others for high unbalances. In Figure 7 the trajectories are plotted for a simple shaft supported in two identical 3-pad tilting pad bearings. The rotor has very large amplitude of triangular motion and the nonlinear behaviour appears clearly. For these operating conditions, the orbit is largely following the bearing geometry. By taking the pad deformation into account, the orbit increases by about 15 % compared to that without deformations. These curves match the calculations of Desbordes et al. ([15], Figure 9) very well.

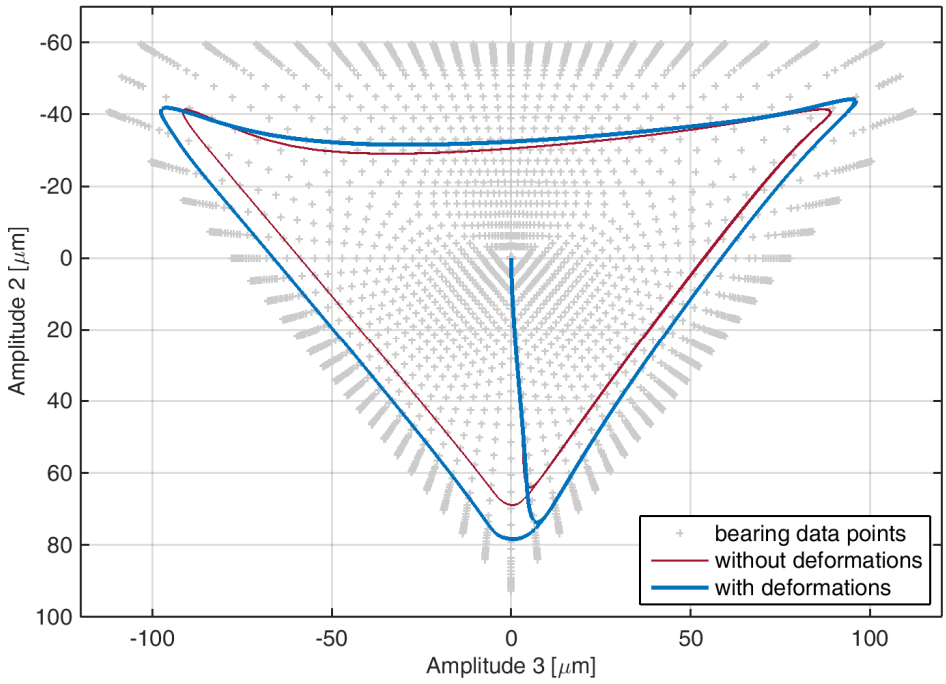

Figure 7: Journal centre orbit for a static load (30 kN) with a high unbalance force (50 kN) in 3-pad tilting pad bearing

For a more precise calculation considering the 3D-Temperature distribution, the turbulent flow regime, time-dependent cavitation boundaries, the computation time increases exponentially and such a calculation of trajectories is limited to exceptional cases. Therefore the components of the transient bearing force $(So_D, \alpha_D, \beta_{ik}^*)$ are precalculated at certain grid points (grey crosses in Figure 7). These grid points are automatically distributed by the program ALP3T2Penhanced, so that nearly 99.99% of the possible shaft deflection is covered . Moreover the change of the Sommerfeld number between two grid points is less than a certain factor.

4 Calculation Results for Squeeze Film Dampers

For a squeeze film damper, the "velocity" is ω=0. By multiplication of equation (6) with ω/ω_S, setting $\omega=0$ and neglecting the inertia forces, only the term $\partial(\rho_{mix}H)/\partial\phi$ remains on the right side of (6). In addition ω_S is used instead of ω to get the dimensionless variables Π and ϕ, and there is no turbulent flow regime in the squeeze film damper. After perturbing equation (6) with equation (10) only the last 2 relations of equation (11) are obtained. In other words the squeeze film damper has only transient forces which are proportional to the vibration velocity and does not create any static force or stiffness unless certain design measures are taken for centring the squeeze ring.

The Sommerfeld numbers So_V calculated with the enhanced program ALP3T2Penhanced (squeeze film damper with 2 phase model) are plotted in comparison to the limit values for the 2π-film (Sommerfeld boundary condition) and the π-film (Gümbel boundary condition), Figure 8. The eccentricity velocity ε' becomes an additional parameter for the pure squeezing movement ($\omega=0, \gamma'=0$) if the oil foaming is considered. The eccentricity velocity determines the cavitation in the squeeze film damper. The calculated So_V-values range between the asymptotical limit values of the π- and 2π-film for a cylindrical 360° squeeze film damper with axial oil supply. The differences between the So_V-values depend strongly on the eccentricity ε of the squeeze film damper for the three calculation models.

The influence of the cavitation is very important for small eccentricities ε, i.e. especially for high speed journal bearings with low load or statically centred squeeze film dampers.

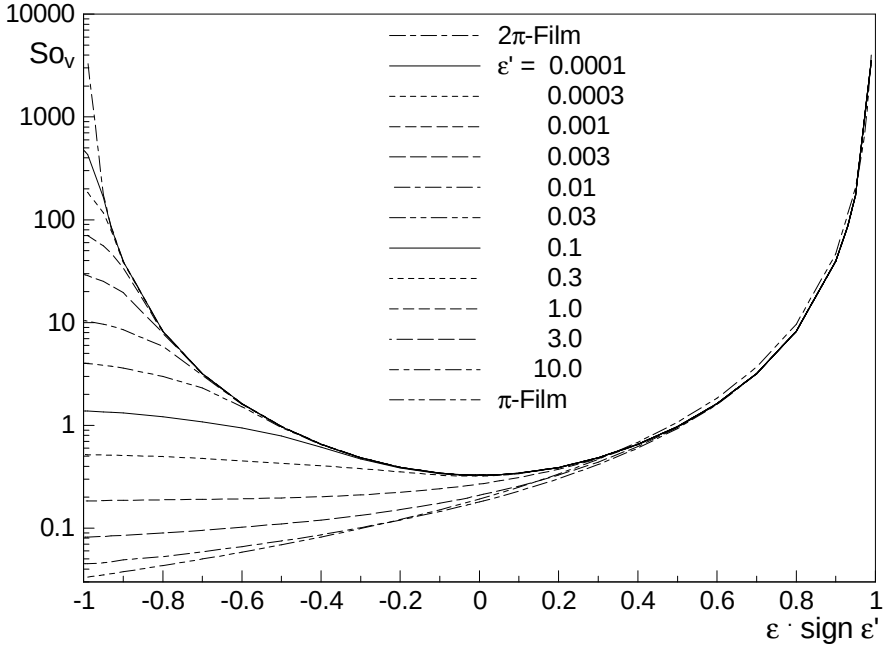

Figure 8: Comparison of the calculated Sommerfeld numbers $So_V(\varepsilon,\varepsilon')$ with Sommerfeld (2π-Film) and Gümbel (π-Film) boundary condition

For a turbocharger with two floating ring bearings with non-rotating rings the trajectories are plotted in Figure 9. The movement of the floating ring itself is shown in the right picture, while the relative shaft to ring vibration is in the left one. The calculation have been started for nominal speed with centred ring and shaft position. The bearing at "C-side" is statically nearly unloaded, while the other bearing has to carry the whole weight of the turbocharger. The shaft and the ring drop down directly after starting the calculation. The inner oil film produces immediately a film pressure due to the rotation of the shaft, whereas the ring must be accelerated to a certain velocity, so that the outer oil film can carry the mass of the ring and the shaft. As the vibration velocity of the ring is increased, the ring starts to centre itself. Sub-synchronous vibrations appear due to the low loading of the bearings.

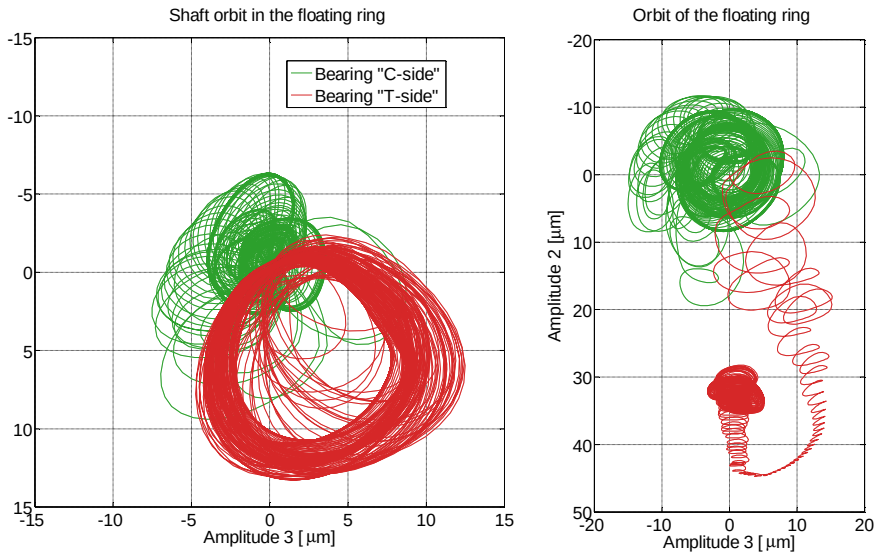

Figure 9: Orbit plots of the squeeze film ring and the shaft relative to the ring in a turbocharger

5 Conclusion

The behaviour of bearings and squeeze film dampers is analysed for static and dynamic loading with the program ALP3T2Penhanced, which considers several additional effects such as oil foaming, turbulence, and inertia. By integrating the program ALP3T2Penhanced into the rotor dynamics program MADYN 2000, the linear and nonlinear vibrations of rotor–bearing–stator systems can be accurately calculated. For squeeze film dampers, the important centring effect due to the dynamic load can be clearly shown by nonlinear analyses with the enhanced program system.

References

[1] Holland, J., Berkowitz, B., Schwarze, H. (1991): Instationär belastete Gleitlager. *Tribologie und Schmierungstechnik* **39**, pp. 94-100.

[2] DIN 31657 (1996): *Hydrodynamische Radialgleitlager im stationären Betrieb. Berechnungsgrundlagen für Mehrflächen- und Kippsegmentlager*. Beuth, Berlin.

[3] Mittwollen, N., Rückert, A., Schmitz, A., Reinhardt, W.-D. (1991): Verbesserung der Berechnungsgrundlagen für schnellaufende hochbelastete Mehrgleitflächen- und Radialkippsegmentlager. Abschlußbericht BMFT-Verbundprojekt „Gleitlageruntersuchungen“ (Teilprojekt 03T0012A). TU Braunschweig.

[4] Meyer, A. (1987): *Äußere Lagerdämpfung für sehr hochtourige, gleitgelagerte Rotoren.* Dissertation U Karlsruhe.

[5] Schmied, J., Perucchi, M, Pradetto, J-C. (2007): Application of MADYN 2000 to rotordynamic problems of industrial machinery. IGTI, GT2007-27302.

[6] Fuchs, A. (2002): *Schnelllaufende Radialgleitlagerungen im instationären Betrieb.* Dissertation TU Braunschweig.

[7] Peeken, H., Benner, J. (1985): Beeinträchtigung des Druckaufbaus in Gleitlagern durch Schmierstoffverschäumung. *VDI-Bericht.* **549**, pp 371–397, VDI, Düsseldorf.

[8] Werner, H. K. (1986): *Schmierstoffe.* Deutsche Shell AG.

[9] Pinkus, O., Sternlicht, B. (1961): *Theory of Hydrodynamic Lubrication.* McGraw-Hill, New York, Toronto, London.

[10] Han, D. C. (1979): *Statische und dynamische Eigenschaften von Gleitlagern bei hohen Umfangsgeschwindigkeiten und bei Verkantung.* Dissertation U Karlsruhe.

[11] Falz, E. (1931): *Grundzüge der Schmiertechnik*. Springer, Berlin.

[12] Rückert, A. (1992): *Experimentelle Überprüfung der Berechnungsgrundlagen für die Radialgleitlager von Turbomaschinen.* Fortschr.-Ber. VDI Reihe 1 **214**, Düsseldorf.

[13] Glienicke, J. (1966): *Feder- und Dämpfungskonstanten von Gleitlagern für Turbomaschinen und deren Einfluß auf das Schwingungsverhalten eines einfachen Rotors.* Dissertation TH Karlsruhe.

[14] Glienicke, J., Fuchs, A., Lutz, M. (1997): *Energetisch gekoppelte, nichtlineare Lagerschmierfilme mit instationären Randbedingungen.* FVV **653**, Frankfurt/M.

[15] Desbordes, H., Fillon, M., Chan Hew Wai, Frene, J (1994); *Dynamic Analysis of Tilting-Pad Journal Bearing – Influence of Pad Deformations*. J. of Trib. **116**, pp. 621-628.